INTERFACE

royalsocietypublishing.org/journal/rsif

Research

Cite this article: Mirbod P, Haffner EA, Bagheri M, Higham JE. 2021 Aerosol formation due to a dental procedure: insights leading to the transmission of diseases to the environment. *J. R. Soc. Interface* **18**: 20200967.
https://doi.org/10.1098/rsif.2020.0967

Received: 28 November 2020
Accepted: 17 February 2021

Subject Category:
Life Sciences–Engineering interface

Subject Areas:
environmental science, medical physics, biomedical engineering

Keywords:
coronavirus, COVID-19, dental procedures, droplet velocity, experiments, size distributions

Author for correspondence:
Parisa Mirbod
e-mail: pmirbod@uic.edu

THE ROYAL SOCIETY PUBLISHING

Aerosol formation due to a dental procedure: insights leading to the transmission of diseases to the environment

Parisa Mirbod[1], Eileen A. Haffner[1], Maryam Bagheri[1] and Jonathan E. Higham[2]

[1]Department of Mechanical and Industrial Engineering, University of Illinois at Chicago, 842 W. Taylor Street, Chicago, IL 60607, USA
[2]School of Environmental Sciences, University of Liverpool, Liverpool, UK

PM, 0000-0002-2627-1971; EAH, 0000-0002-8284-958X; JEH, 0000-0001-7577-0913

As a result of the outbreak and diffusion of SARS-CoV-2, there has been a directive to advance medical working conditions. In dentistry, airborne particles are produced through aerosolization facilitated by dental instruments. To develop methods for reducing the risks of infection in a confined environment, understanding the nature and dynamics of these droplets is imperative and timely. This study provides the first evidence of aerosol droplet formation from an ultrasonic scalar under simulated oral conditions. State-of-the-art optical flow tracking velocimetry and shadowgraphy measurements are employed to quantitatively measure the flow velocity, trajectories and size distribution of droplets produced during a dental scaling process. The droplet sizes are found to vary from 5 µm to 300 µm; these correspond to droplet nuclei that could carry viruses. The droplet velocities also vary between 1.3 m s^{-1} and 2.6 m s^{-1}. These observations confirm the critical role of aerosols in the transmission of disease during dental procedures, and provide invaluable knowledge for developing protocols and procedures to ensure the safety of both dentists and patients.

1. Introduction

A global pandemic emerging from a novel strain of severe acute respiratory syndrome coronavirus (SARS-CoV-2), namely COVID-19, has ravaged the world throughout 2020. This human-to-human disease is spread by either blood or saliva droplets entrained into aerosols by coughing, sneezing or other means. While the use of face coverings and face shields might reduce transmission in public and general day-to-day life, in professions such as dentistry the transmission of bodily fluids is almost unavoidable [1–3]. Such transmissions have been well documented; accordingly, the *Dental Research Journal* and the US Department of Labor have assessed dentistry as one of the most hazardous occupations with a high risk of exposure to infections such as COVID-19 [4,5].

The arsenal of a typical dentist comprises a variety of high-speed drilling, cleaning and scaling instruments. These instruments use water and compressed air that combine with saliva and even blood, creating aerosols that potentially carry viral particles [6]. Ideally, during a global pandemic, all dentistry employing aerosol-producing tools would cease, but, in reality, this is simply not feasible, as a lack of treatment can also pose risks; for example, a dental abscess caused by a small infection can lead to sepsis and even death [7]. In a recent report, the World Health Organization (WHO) acknowledged the need for dental work to continue and highlighted that this necessitates the use of aerosol-producing tools [8,9]. Also, some other recent studies suggested the use of new suction systems and an Er:YAG laser, as well as the correct application of a disinfectant in order to improve biological safety in the dental clinic/office especially during the COVID-19 pandemic [10,11].

Most worryingly, in the context of an airborne virus, previous dental studies [12,13] have shown that aerosols created by dental devices contain droplets so small that they can stay airborne for extended periods and that these aerosols contain large distributions of droplet sizes. On average, these particles have been found to feature diameters of 50 µm and less than 10 µm, which can penetrate deep into the respiratory system [14,15]. These droplet distributions also contain diameters greater than 50 µm; unfortunately, these droplets 'splatter' and pose significant transmission risks [16–18]. Moreover, particles that splatter and land on surfaces are prone to further evaporation and delayed entrainment of the virus into the air [15]. However, these aerosol transmission mechanisms are not exclusive to COVID-19; they also apply to viruses such as influenza, human immunodeficiency virus (HIV) and even future novel viruses [18,19]. To understand the transmission of the virus, we first need to understand the dynamics of the aerosol surrogate, based upon which it will be possible for dental procedures to be modified and developed to mitigate or minimize transmission.

In this study, we use state-of-the-art experimental fluid mechanics tools, namely optical flow tracking velocimetry (OFTV) and shadowgraphy, to investigate the original formation of droplets created by a Cavitron Select SPS Ultrasonic Scaler (CUS) during the scaling process. Several researchers have previously examined the sizes of droplets using various methods during sneezing, coughing, talking and breathing [20–31]. However, to the best of the authors' knowledge, this study is the first of its kind to investigate droplet nuclei size and velocity distribution in detail using quantitative methods and the implementation of dental instruments. The data obtained in this work (both droplet size and flow-field characteristics) can be employed to quantify the amount of virus that will be transmitted to a receiver in a poorly ventilated space and also to provide a measure of the risk of infection. Thus, they have the potential to be used as guidance to further model (using numerical simulations) how airborne particles are transported into the environment and the human respiratory system and to advance our understanding of how aerosols are transmitted in dental clinics/offices, healthcare centres and hospitals.

2. Material and methods

For our quantitative measurements, we used two tools commonly used in fluid mechanics: (i) to determine the velocity fields and Lagrangian paths of droplets, we used OFTV and (ii) to determine the size of individual droplets, shadowgraphy was employed.

2.1. Optical flow tracking velocimetry

OFTV is a commonly used method in fluid mechanics [32–36]. This method is used to determine the motion of features from a set of high-speed videos. In our case, we used OFTV to track individual droplets created by the CUS; however, the aerosol plume created by the CUS is fully three-dimensional (3D). Using a 1 mm laser sheet created by a 527 nm Nd:YLF (DM20–527; Photonics Industries) laser, we were able to illuminate a single plane inside the aerosol, providing us with a two-dimensional (2D) slice. Using a high-speed camera (Phantom) equipped with a Nikon lens with a focal length of 60 mm, we were further able to capture the reflections from the water droplets. We considered two different planes, P_1 and P_2, as shown in figure 1*b*,*c*. One plane, P_1, is parallel to the tip of the CUS, and the other plane, P_2, is perpendicular to the tip. In each case, to ensure that the mean velocities were fully resolved, 3000 images were collected, resolving more than 100 integral time scales. We also measured the flow rate of the CUS using a plastic bag and an electronic balance with a high precision; we characterized our analysis based on a flow rate of 29.5 ml min^{-1}, which is higher than that typically used in dentistry operations.

The OFTV method is based on solving sets of linear equations (i.e. the optical flow equations), reducing the computational complexity. There are two primary steps involved in OFTV: the first step is determining the features to track, and the second step is tracking them across frames. In this work, we employed the commercial code known as flowonthego. Flowonthego uses eigenfeatures to determine 'features' from the image gradients. These eigenfeatures are determined by first constructing a correlation matrix defined as

$$M = \begin{bmatrix} \Psi_x^2 & \Psi_x \Psi_y \\ \Psi_y \Psi_x & \Psi_y^2 \end{bmatrix}, \tag{2.1}$$

where $\Psi(x,y;\, t)$ is the pixel intensity and Ψ_x and Ψ_y are the intensity gradients in the x- and y-directions, respectively. Gradients are computed from a smoothed field using a Gaussian kernel with a width of five pixels. A response value, R, is taken as the minimum of the two eigenvalues of the correlation matrix given by

$$R = \min\,[\lambda_1, \lambda_2], \tag{2.2}$$

where

$$det[M - \lambda I] = 0. \tag{2.3}$$

In flowonthego, λ_i features are defined as regions with $R > 0.01$. The displacements of features are calculated based on the assumption that the spatial displacements between frames are sufficiently small such that $\Psi(x,y;\, t)$ can be expressed as

$$\Psi(x,y;\, t) = \Psi(x + \delta x,\, y + \delta y;\, t + \delta t). \tag{2.4}$$

Following a Taylor expansion, the above equation can then be rearranged to give the optical flow equation as

$$\Psi_t + u\Psi_x + v\Psi_x \cong 0, \tag{2.5}$$

where Ψ_t is the partial derivative of the pixel intensity with respect to time between image pairs and u and v are the velocities in the x- and y-directions, respectively. The optical flow equation is an underdetermined equation with two unknowns, u and v. A variety of methods can be used to resolve this challenge. The Lucas–Kanade solution method [34,37] is applied to solve the optical flow equations in flowonthego. The Lucas–Kanade approach assumes that the velocity gradients are relatively small; i.e. the velocity at one location is the same as that at its neighbours. Then, a system of optical flow equations can be constructed for each feature as

$$u\Psi_x(x + i, y + j) + v\Psi_y(x + i, y + j) = -\Psi_t(x + i, y + j), \tag{2.6}$$

where i and j define the neighbourhood around the feature at pixel x, y. In our application, we used a neighbourhood of 11; that is, i and j ranged from −5 to +5. This setting allowed us to solve the equation using a least squares method and determine u and v as follows:

$$\begin{bmatrix} u \\ v \end{bmatrix} = \begin{bmatrix} \sum_{i,j} \Psi_x^2 & \sum_{i,j} \Psi_x \Psi_y \\ \sum_{i,j} \Psi_y \Psi_x & \sum_{i,j} \Psi_y^2 \end{bmatrix}^{-1} \begin{bmatrix} \sum_{i,j} \Psi_x \Psi_t \\ \sum_{i,j} \Psi_y \Psi_t \end{bmatrix}. \tag{2.7}$$

Once u and v have been located, we can use these to construct Lagrangian streamlines; alternatively, we can use a gridded interpolator to create a velocity field and scale the fields using a calibration plate [38].

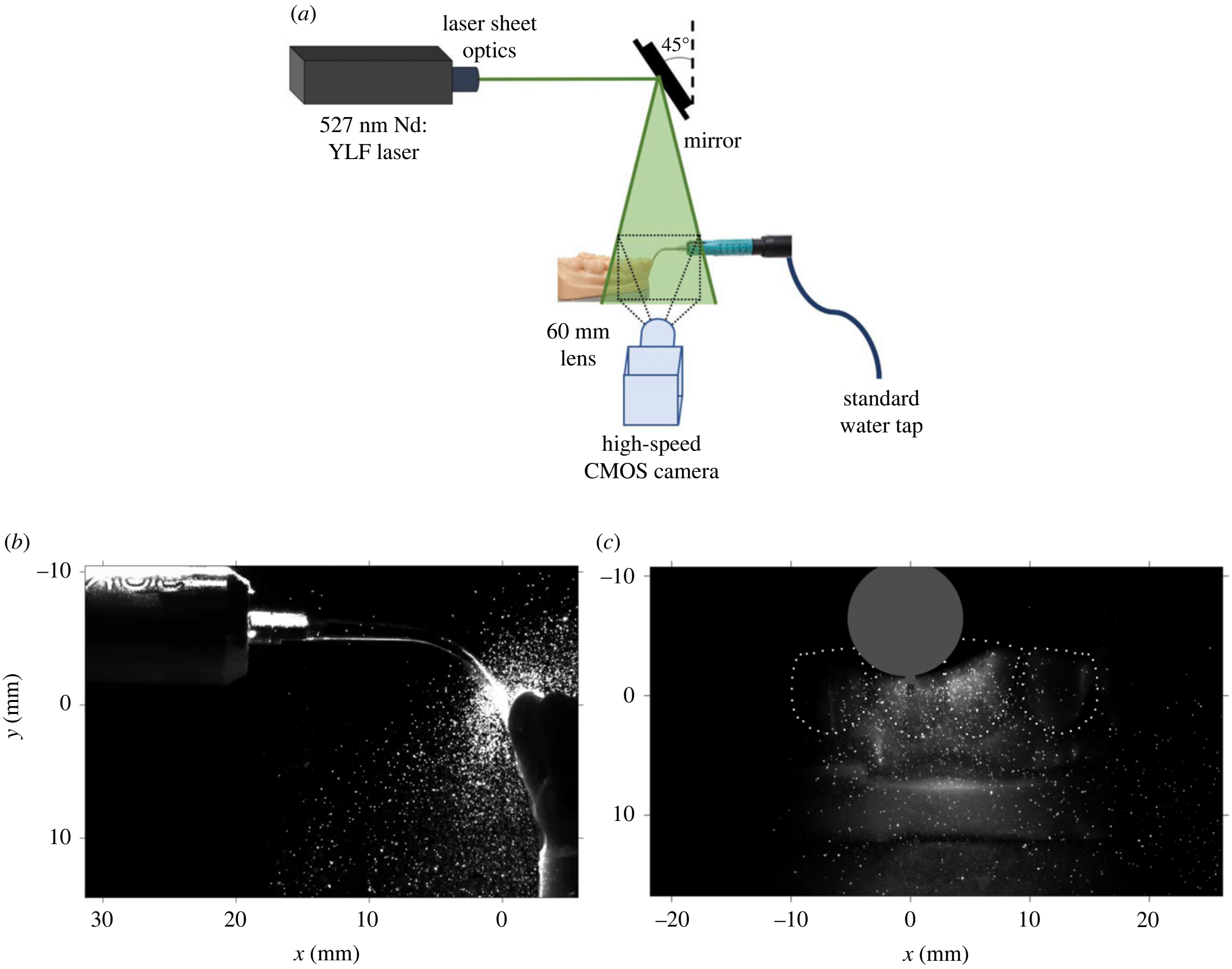

Figure 1. Experimental procedures to detect aerosol formation by a CUS. (*a*) Set-up schematic for the OFTV technique to detect the droplet velocity and Lagrangian path. Examples of the raw OFTV images in the (*b*) P_1 plane and (*c*) P_2 plane recorded with a high-speed camera at 7.6 kHz.

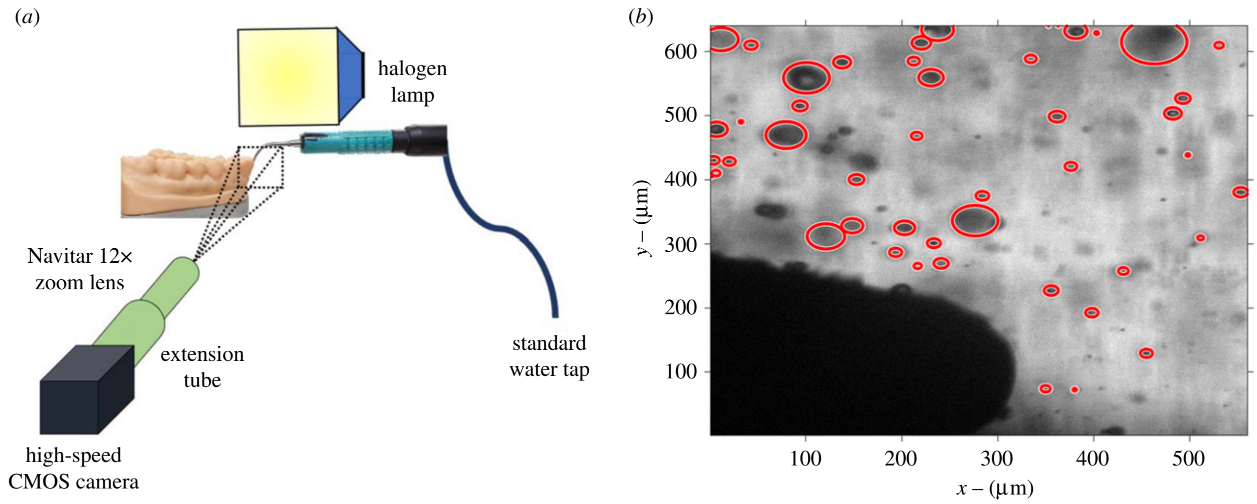

Figure 2. (*a*) Schematic of the experimental set-up of backlight illumination for the shadowgraphy technique. (*b*) An example of backlight illumination at 0.08 s recorded using a high-speed camera at 7.6 kHz and two halogen backlights.

2.2. Shadowgraphy and particle identification

Shadowgraphy is a well-used technique in fluid mechanics that allows us to quantitively visualize small droplets using simple optics [36]. To create these visualizations, we used a high-magnification camera lens and backlight illumination from a halogen lamp (figure 2). The measurement plane is defined by the camera depth of focus in the focal plane. In our set-up, we used a Navitar zoom lens (Thorlabs, Inc.) attached to the high-speed Phantom camera set to an exposure rate of 20 µs. This allowed us to zoom into a small region (approx. 100 µm thick) to accurately measure the size of small droplets of the order of 5 µm (figure 2). From the raw images, we used an in-house

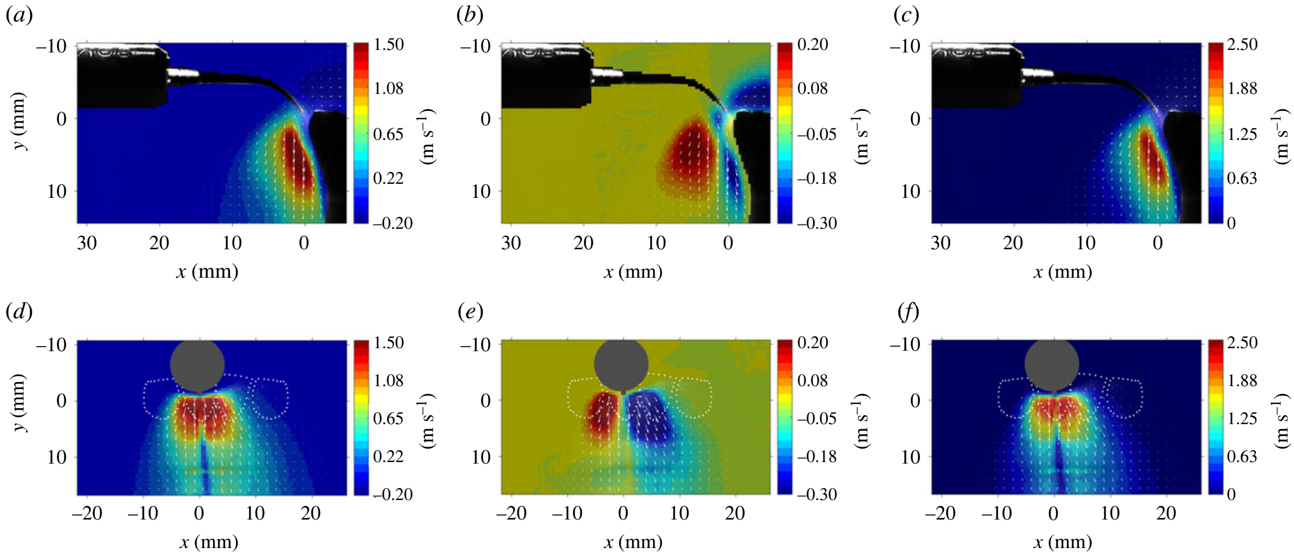

Figure 3. The mean field of the (*a*) V (*y*-axis) velocity component, (*b*) U (*x*-axis) velocity component and (*c*) velocity magnitude for the plane parallel to the CUS tip, P_1, and the (*d*) V (*y*-axis) velocity component, (*e*) U (*x*-axis) velocity component and (*f*) velocity magnitude for the plane perpendicular to the CUS tip, P_2. The white arrows in the figures specify the velocity vectors.

detection code to determine the size and location of each droplet. The code works by first binarizing the raw image based on an adaptive threshold. Using an adaptive Hough transform [39], we then determined circular regions, i.e. droplets, and defined the velocity of the droplets using OFTV. However, instead of using the eigenfeatures for droplet detection, we employed the centroids determined by the Hough transform.

3. Results

In this study, we investigate the aerosols produced by a CUS manufactured by Dentsply International, PA, USA. We simulate a patient's mouth using a mandible set of teeth, as shown in figures 1 and 2. The CUS usually has different scalar tips designed for use in different areas of the patient's teeth. Herein, a Slimline SLI 10 L 30 K ultrasonic insert was fitted onto the CUS to study the effect of the spray on the front teeth of the patient. As in routine dental practice, the tip of the Slimline was placed perpendicular to the front lower teeth pointing towards the gum line (figure 1) and remained in the same position for all of the experiments. The CUS was connected to a standard water tap (20–40 psi) within the laboratory. In the experiments, we set the flow rate to 29.5 ml min^{-1}, a typical flow rate used in practice.

3.1. Global droplet velocity contours

Figure 3 shows the global velocity components (U, V and magnitude) for the planes both parallel and perpendicular to the teeth, i.e. planes P_1 and P_2, respectively, obtained from OFTV. Figure 3*a*,*d* demonstrate that the maximum U velocity of 1.5 m s^{-1} occurs near the tip of the CUS close to the front teeth, while it is reduced far from the tip. The mean V velocity is the lowest at 0.2 m s^{-1} compared with the mean maximum velocity (2.5 m s^{-1}) of the magnitude velocity profile, as can be seen in figure 3*b*,*c*,*e*,*f*. The spray breaks up at a distance of approximately 10 mm from the teeth, where the magnitude of the velocity almost disappears. The splatter attains a cone shape before breaking up further from the tip; at the break-up location (approximately 10 mm from the teeth), the cone disintegrates into droplets and aerosols with reduced velocities. The continuous break-up of droplets into smaller sizes and aerosols is apparent further from the teeth. Furthermore, a myriad of other droplets are detected owing to the ejection of the water from the CUS device.

The temporal evolution of close-up snapshots of the splatter velocity magnitude at various times for the (*a*,*b*,*c*) P_1 plane and (*d*,*e*,*f*) P_2 plane are presented in figure 4. Here, the duration of the CUS operation is approximately 100 ms. Our experiments reveal that, first, a large droplet is produced at the tip of the CUS with a diameter of approximately 330 µm, as observed in figure 5*a* (the figure represents a selection of all obtained images); however, this large droplet bursts, on average, after 57 ms, generating a huge number of droplets of various sizes. A sequence of splatter formation at (*a*) 0.04 s, (*b*) 0.08 s and (*c*) 0.12 s during the CUS operation can be observed in figure 5*a*–*c*. It should be noted that the size of this large droplet depends on the flow rate (i.e. the setting at which the CUS is operated). The droplet trajectories representing 20% of the detected droplets for both the P_1 and the P_2 planes acquired using OFTV are also shown in figure 6. The colour bars represent the individual droplets' velocity magnitude, which varies in the field of view. The maximum speed, corresponding to the local or individual measurements, of the droplets is approximately 2.6 m s^{-1}, and most of the droplets are large enough to settle quickly. We even observed droplets at a distance of approximately 9 mm from the CUS tip; these droplets are either very small in size or evaporate rapidly, producing droplet nuclei. These droplets could be responsible for the transmission of viruses to the respiratory system.

To further characterize the droplet size distribution produced after the break-up of the largest droplet, we employed the shadowgraphy technique. As shown in figure 7*a*,*b*, we measured droplet sizes ranging from 5 µm to 500 µm with a maximum observed speed of 2.6 m s^{-1}. It should be noted that the size and velocity distributions of the individual droplets depend strongly on the flow rate at which the CUS device operates. In addition, the person's mouth and the particular tooth targeted by the CUS might affect this distribution. While the size distribution of respiratory droplets has been the subject of a number of studies (e.g.

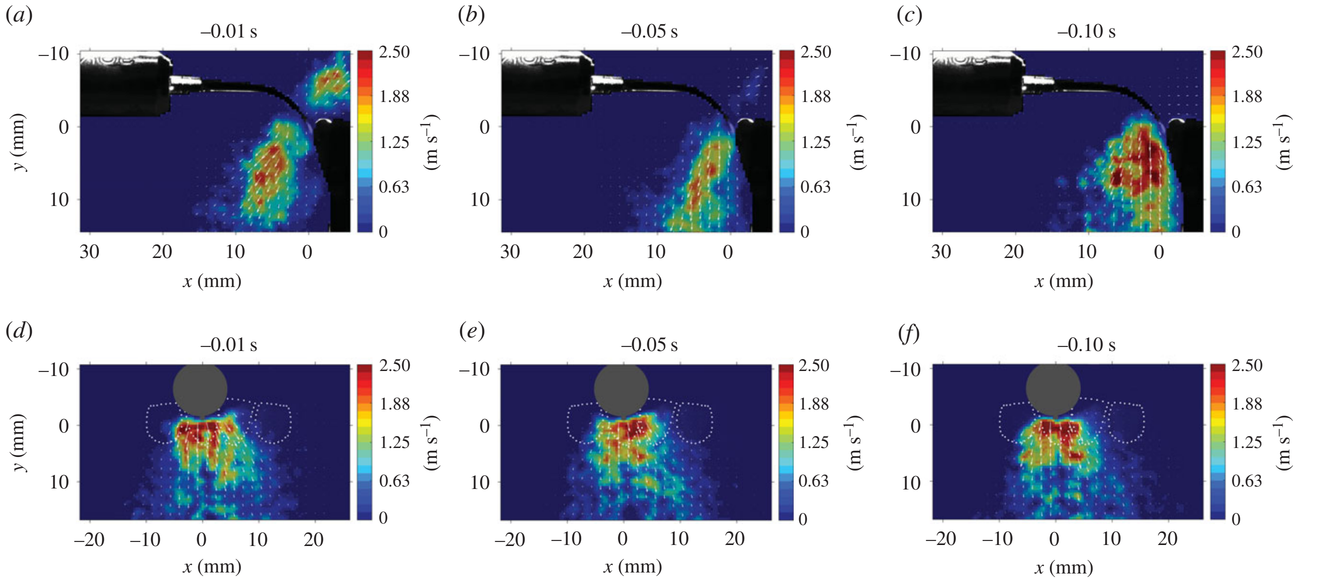

Figure 4. Temporal evolution of the velocity magnitude of the splatter for the P_1 plane at (*a*) 0.01 s, (*b*) 0.05 s and (*c*) 0.10 s and for the P_2 plane at (*d*) 0.01 s, (*e*) 0.05 s and (*f*) 0.10 s. The white arrows in the figures specify the velocity vectors.

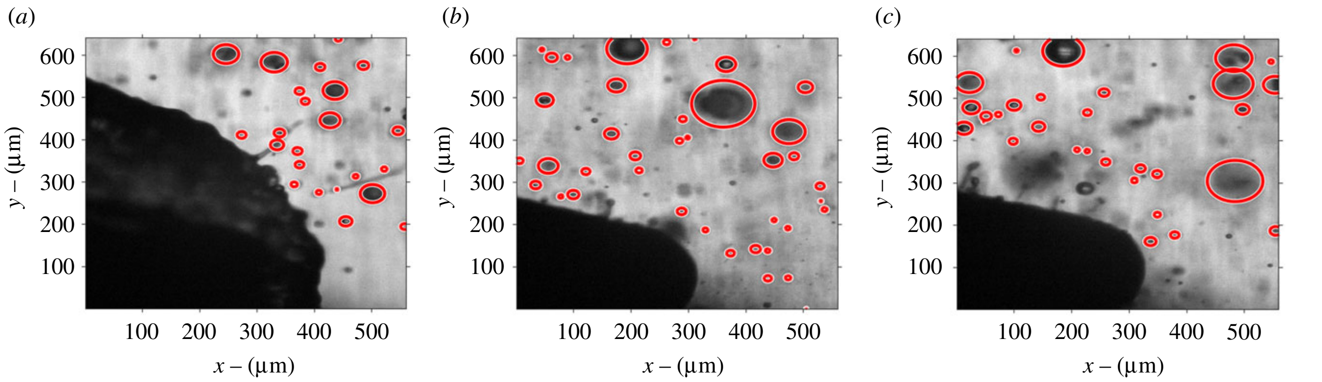

Figure 5. Sequences of splatter formation at (*a*) 0.04 s, (*b*) 0.08 s and (*c*) 0.12 s. Image samples were recorded using a high-speed camera at 7.6 kHz and two halogen backlights.

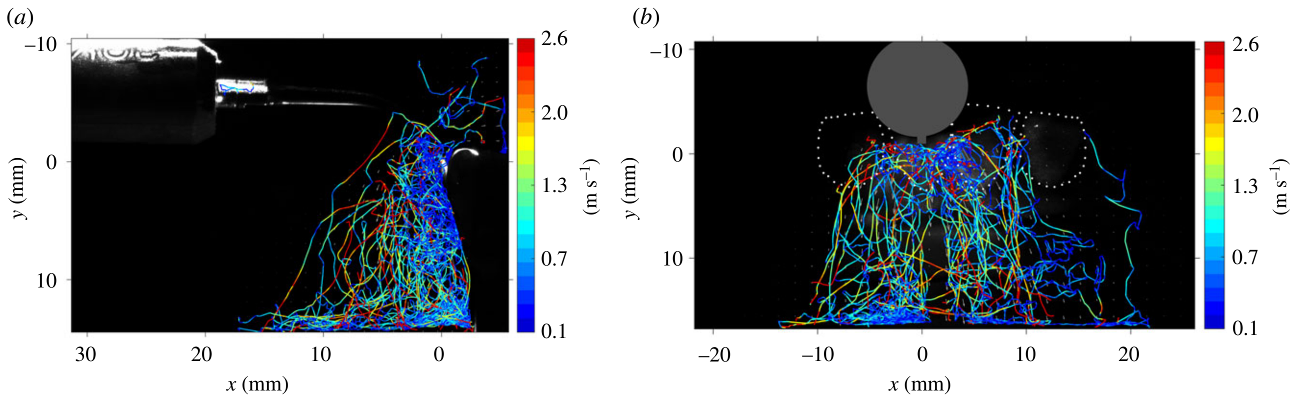

Figure 6. Droplet trajectories representing 20% of the detected droplets for the (*a*) P_1 plane and (*b*) P_2 plane.

[20]), with increasing focus on improving the measurement precision in the small submicron range (e.g. [24,26,27]), to the best of the authors' knowledge, the size and velocity distributions of the droplets produced by the CUS have not been characterized in detail previously. Generally, it is assumed that smaller droplets and particles penetrate the respiratory tract and reach deeper target tissues within the lungs. Besides, experiments on animals using respiratory pathogens and solid particles suggest that inhalation of an atomized solution increases the infection and death rates compared with direct intranasal inoculation (e.g. [40,41]). Our results confirm that small droplet sizes are indeed produced during dental procedures, including those involving a CUS. Although wearing masks can filter droplets and

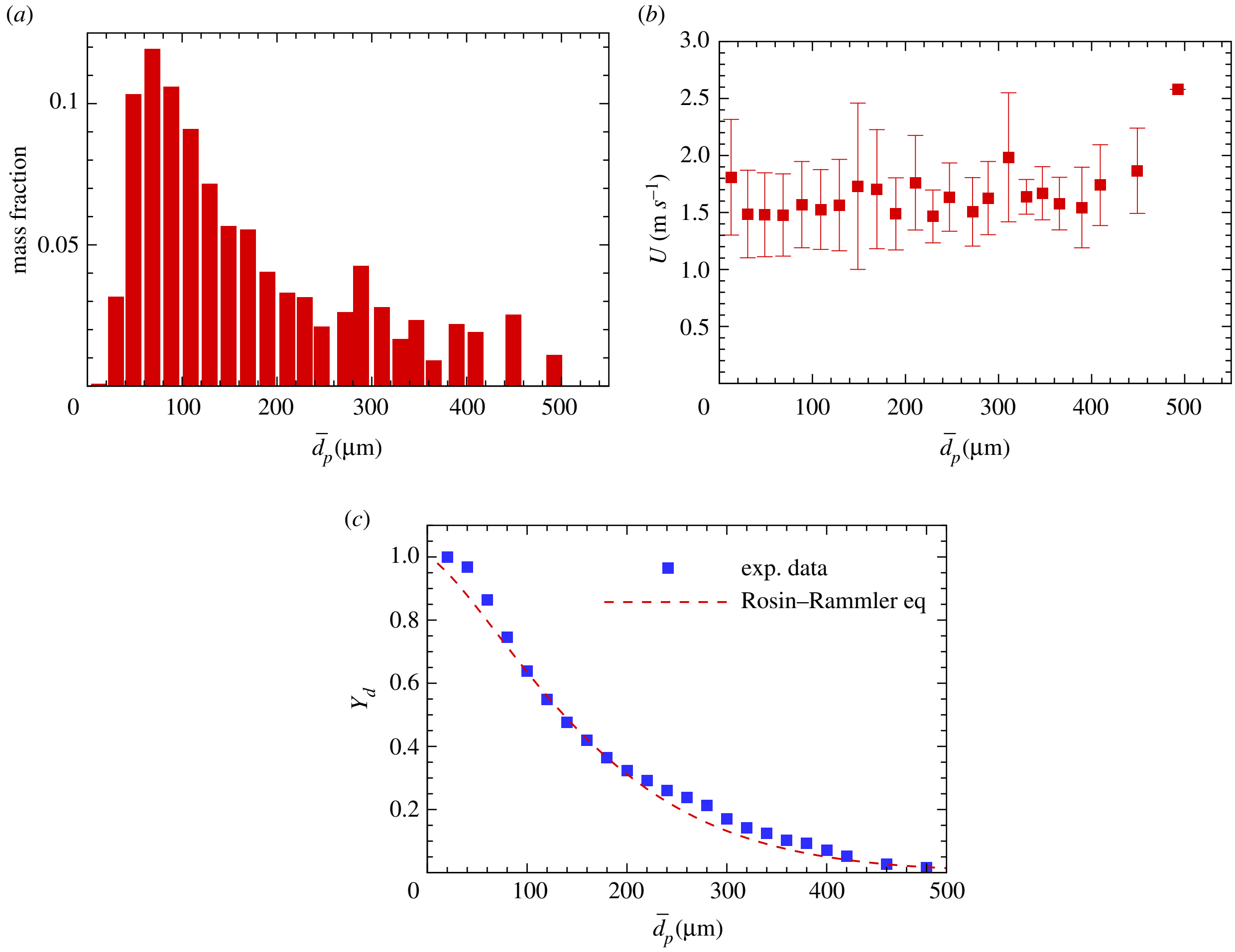

Figure 7. (*a*) Histogram of the droplet size distribution. (*b*) The velocity distribution of the droplets. (*c*) The Rosin–Rammler curve fitted for our obtained experimental droplet size data with a 29.5 ml min^{-1} flow rate.

aerosols, mitigating against the transmission of airborne pathogens, new protocols must be considered in dental clinics/offices, healthcare centres and hospitals to further decay these transmissions into the environment.

Moreover, we compared our experimentally obtained data with the Rosin–Rammler equation [42]. The Rosin–Rammler size distribution is a well-known distribution function and a convenient representation of the droplet size distribution for liquid sprays. In particular, this fitting can be used as an initial condition in numerical simulations to further model how droplets are transmitted to the environment, including dental clinics/offices. This distribution can also be used in a broad array of applications ranging from bioproduct development [43] to the break-up of liquid droplets (e.g. in spray technology [44]) and aerosol science [45].

The Rosin–Rammler distribution function assumes that an exponential relationship exists between the droplet diameter d_p and the mass fraction of droplets with a diameter greater than d_p that can be defined as $Y_d = e^{-(d/\bar{d})^n}$, where $\bar{d}$ is the size constant (mean diameter) and n is the size distribution parameter (spread parameter). We found $\bar{d}$ and n as 178.8 µm and 1.36, respectively, by applying the Rosin–Rammler fit to the data. Our results show very good agreement with the mathematical model proposed by the Rosin–Rammler size distribution.

To generalize the problem and to characterize the break-up of the fluid in more detail, we also examined some dimensionless parameters, for which we measured the characteristic length to be the CUS tip diameter, $d = 635$ µm. We defined the Reynolds number as $Re = u_o\rho_f d/\mu_f$, where u_o is the initial velocity as it leaves the tip of the device, which was determined from the flow rate, and ρ_f and μ_f are the density and the viscosity of the fluid, respectively. Water is considered in this study to be at room temperature (20°C), where $\rho_f = 0.998\ \mathrm{g/cm^3}$ and $\mu_f = 0.001$ Pa.s. The Weber number can then be defined as $We = \rho_f u_o^2 d/\sigma$, where σ is the surface tension of water [46] and the resulting Ohnesorge number is $Oh = \mu_f/\sqrt{\rho_f d\sigma} = \sqrt{We}/Re$ [28]. To calculate the Stokes number, which is responsible for the settling of droplets, the relaxation time (which depends on the average droplet diameter) needs to be determined first. The relaxation time is reported as $\bar{\tau}_o = \rho_f \bar{d}_p^2/18\mu_g$, where $\mu_g = 1.82 \times 10^{-5}$ Pa.s is the viscosity of the surrounding gas (air in this study) and the average droplet diameter $\bar{d}_p$ can be determined using shadowgraphy. The Stokes number can then be defined as $St = \bar{\tau}_o u_o/d$ [47]. Table 1 reports the resulting dimensionless parameters of the current study. For comparison, the values computed for coughing and sneezing are also shown in table 1. Comparing the dimensionless parameters from our experiments with those produced by coughing and sneezing confirms that our reported values are much lower than the values associated with coughing/sneezing [28,46–49]. This is because the flow rate in which the CUS operates is much lower, resulting in a laminar flow regime compared with the coughing/sneezing where the flow is turbulent; therefore, the related values would be higher. On the other hand, our data produce smaller

Table 1. The experimental parameters for the different tests conducted at 20°C. The dimensionless parameters remained constant throughout all experiments. The second row represents the values reported for coughing and sneezing.

	flow rate (ml min^{-1})	u_o (cm s^{-1})	*Re*	*We*	*Oh*	$\bar{\tau}_o$	St
aerosol formation by the CUS	29.5	4.92	31.19	0.02	4.7×10^{-3}	7.55×10^{-3}	0.57
coughing/ sneezing	9.6×10^4–5.1×10^5 [48]	coughing: 112 [48] sneezing: 220	coughing: 10^4 [49] sneezing: 4×10^4 [49]	sneezing: 2.2 [28]	sneezing: <1 [28]	—	—

size drolpets, which results in taking precautions for those who are exposed to these droplets.

4. Discussion

In this study, we performed the very first quantitative analysis of the size and velocity distributions of the droplet nuclei produced by a CUS in a setting common to dental clinics. We carried out a series of experiments using state-of-the-art techniques, namely OFTV and shadowgraphy. We applied OFTV to measure the global velocity of the droplets and used shadowgraphy to measure the number, size, shape and speed of individual droplets produced by the CUS. Specifically, the experiments in this study were carried out on the front teeth, where we found the maximum number of droplets and occurrences of splatter moving out of the mouth. Depending on the flow rate, the droplet sizes ranged from 5 µm to 500 µm. As the flow rate increased, smaller droplets were produced, and their velocity decreased.

To compare the obtained data with previous works using coughing, sneezing and speaking and to further examine the transmission of droplets in the environment, we also computed some dimensionless parameters, including the Reynolds and Stokes numbers. In general, the values obtained of the droplet nuclei produced by a CUS are much lower than those of coughing and sneezing. At low Reynolds and low Stokes numbers, similar to the findings of this study, the Stokes settling speed of a droplet in an ambient gas phase is proportional to its surface area, which decreases with time owing to evaporation; therefore, we could treat the aerosol particles as passive tracers that follow the flow because they stay longer in the environment and could be more dangerous. It should be emphasized that the role of airborne transmission in the respiratory disease was first examined by Wells [41,50], who compared the complete evaporation time with the settling time of different droplets with diameters ranging from 1 µm to 1000 µm. He found that droplets with diameters of d>100 µm settle to the ground in less than 1 s without significant evaporation, whereas droplets with d < 100 µm will typically become droplet nuclei before settling [41]. Droplets with d < 5–10 µm rapidly evolve into droplet nuclei with settling speeds of less than 3 mm s^{-1}; therefore, these droplets (similar to our findings) could become suspended and advected by a cloud of air emitted by the environment or resuspended by any ambient flow that may arise, for example, through air conditioning. Considering this analysis and also since our experiments were performed at a relative humidity of 25% and a temperature of 20°C, one expects that the droplets would evaporate in a few seconds. We estimated that for a 2 µm droplet size, the evaporation time is approximately 1 ms [51]; consequently, the suspended droplet nuclei produced by a CUS are expected to be critical elements in long-range airborne transmission; for example, these droplet nuclei could be inhaled by others, thereby stimulating new SARS-CoV-2 infections. Compared with coughing/sneezing or talking, although the amount of virus is possibly lower in smaller droplets produced from dental procedures or the droplets which contain relatively more water, the pathogenic microorganisms can be yet transmitted through inhalation of airborne microorganisms that can remain suspended in the air for a long period of time. When dental devices operate in the patient's mouth, with the existence of the external water jet, a large amount of aerosol and droplets mixed with the patient's saliva or even blood will be formed. These droplets and aerosols are small enough to stay airborne for an extended period before they settle on surfaces or enter the respiratory tract [1].

To summarize, the data obtained in this work are timely and can serve as a guidance to further model (using numerical methods [52,53]) the transmission of airborne particles to humans and to advance our understanding of how aerosols are transmitted in dental clinics/offices, healthcare centres and hospitals. Similar estimates and guidelines for the importance of contact time have been proposed recently for ventilated spaces, based on well-mixed models [54]. These experimental results can be used not only for COVID-19, which has the potential to spread through droplets and aerosols from infected individuals, but also for other viruses, including HIV, hepatitis B and influenza, all of which are possible hazards that a dental worker or patient can encounter in a dental clinic.

The experimental techniques can also be employed as a technique to directly measure the droplet size and distributions in coughing, sneezing, talking and speaking [30,31] as there are already several studies that examined the droplet size distribution using indirect measurements where they all have their own restrictions [31]. It should also be noted that the splatters and droplets formed by the CUS are generally composed of suspended droplets of varying sizes and of the surrounding atmosphere, which is hot/cold and moist. These splatters and droplets also contain saliva and blood, which may change the results. For example, in a recent study on coughing/sneezing [55], researchers found that, by considering the lips and saliva, a thin film of lubricating saliva spreads across the lips resulting in different splatter formation and droplet size distributions. The shape and orientation of patients' lips might also impact the flow and droplet distributions. These are all the subject of further investigations.

Data accessibility. The codes and data used to generate the results in the paper are available at https://doi.org/10.5061/dryad.34tmpg4jq.

Authors' contributions. P.M. designed the research; E.A.H., M.B. and J.E.H. performed the research; P.M. and J.E.H. analysed the data; and P.M., E.A.H. and J.E.H. wrote the paper.

Competing interests. We declare we have no competing interests.

Funding. This work was funded by the University of Illinois at Chicago (UIC) – College of Dentistry (grant no. 200258-323152).

References

1. Peng X, Xu X, Li Y, Cheng L, Zhou X, Ren B. 2020 Transmission routes of 2019-nCoV and controls in dental practice. *Int. J. Oral Sci.* **12**, 1–6. (doi:10.1038/s41368-020-0075-9)
2. Wei J, Li Y. 2016 Airborne spread of infectious agents in the indoor environment. *Am. J. Infect. Control* **44**, S102–S108. (doi:10.1016/j.ajic.2016.06.003)
3. Volgenant CM, Persoon IF, de Ruijter RA, de Soet J. 2021 Infection control in dental health care during and after the SARS-CoV-2 outbreak. *Oral Dis.* **27(Suppl. 3)**, 674–683. (doi:10.1111/odi.13408)
4. Ayatollahi J, Ayatollahi F, Ardekani AM, Bahrololoomi R, Ayatollahi J, Ayatollahi A, Owlia MB. 2012 Occupational hazards to dental staff. *Dent. Res. J.* **9**, 2. (doi:10.4103/1735-3327.92919)
5. OSHA. 2020 *U.S. Department of labor issues alert to help keep dental industry practitioners safe during the coronavirus pandemic*. Washington, DC: The U.S. Department of Labor's Occupational Safety and Health Administration (OSHA).
6. Cleveland JL, Gray SK, Harte JA, Robison VA, Moorman AC, Gooch BF. 2016 Transmission of blood-borne pathogens in US dental health care settings: 2016 update. *J. Am. Dent. Assoc.* **147**, 729–738. (doi:10.1016/j.adaj.2016.03.020)
7. Shweta S. 2013 Dental abscess: a microbiological review. *Dent. Res. J.* **10**, 585.
8. CDC and ICAN. 2019 *Best practices for environmental cleaning in healthcare facilities in resource-limited settings*. Atlanta, GA: US Department of Health and Human Services, CDC; Cape Town, South Africa: Infection Control Africa Network. See https://www.cdc.gov/hai/prevent/resourcelimited/environmental-cleaning.html and http://www.icanetwork.co.za/icanguideline2019.
9. World Health Organization. Considerations for the provision of essential oral health services in the context of COVID-19. Interim guidance. 3 August, 2020. See https://www.who.int/publications/i/item/who-2019-nCoV-oral-health-2020.1.
10. Matys J, Grzech-Leśniak K. 2020 Dental aerosol as a hazard risk for dental workers. *Materials* **13**, 5109. (doi:10.3390/ma13225109)
11. Matys J, Grzech-Leśniak K, Dominiak M. 2020 Disinfectants and devices for surface and air disinfection in dental offices. *J. Stomatol.* **73**, 200–205. (doi:10.5114/jos.2020.98267)
12. Bennett A, Fulford M, Walker J, Bradshaw D, Martin M, Marsh P. 2000 Microbial aerosols in general dental practice. *Br. Dent. J.* **189**, 664–667. (doi:10.1038/sj.bdj.4800859)
13. Nikitin N, Petrova E, Trifonova E, Karpova O. 2014 Influenza virus aerosols in the air and their infectiousness. *Adv. Virol.* **2014**, 859090. (doi:10.1155/2014/859090)
14. Micik RE, Miller RL, Mazzarella MA, Ryge G. 1969 Studies on dental aerobiology: I. Bacterial aerosols generated during dental procedures. *J. Dent. Res.* **48**, 49–56. (doi:10.1177/00220345690480012401)
15. Harrel SK, Molinari J. 2004 Aerosols and splatter in dentistry: a brief review of the literature and infection control implications. *J. Am. Dent. Assoc.* **135**, 429–437. (doi:10.14219/jada.archive.2004.0207)
16. Hinds WC. 1999 *Aerosol technology: properties, behavior, and measurement of airborne particles*. New York, NY: John Wiley & Sons.
17. Cottone JA, Terezhalmy GT, Molinari JA. 1991 *Practical infection control in dentistry*, pp. 139–140. Philadelphia, PA: Lea & Febiger.
18. Monaghan N. 2016 Emerging infections–implications for dental care. *Br. Dent. J.* **221**, 13–15. (doi:10.1038/sj.bdj.2016.486)
19. Smales F, Samaranyake L. 2003 Maintaining dental education and specialist dental care during an outbreak of a new coronavirus infection. Part 1: a deadly viral epidemic begins. *Br. Dent. J.* **195**, 557–561. (doi:10.1038/sj.bdj.4810723)
20. Duguid J. 1946 The size and the duration of air-carriage of respiratory droplets and droplet-nuclei. *Epidemiol. Inf.* **44**, 471–479. (doi:10.1017/S0022172400019288)
21. Loudon RG, Roberts RM. 1967 Droplet expulsion from the respiratory tract. *Am. Rev. Respir. Dis.* **95**, 435–442.
22. Papineni RS, Rosenthal FS. 1997 The size distribution of droplets in the exhaled breath of healthy human subjects. *J. Aerosol Med.* **10**, 105–116. (doi:10.1089/jam.1997.10.105)
23. Nicas M, Nazaroff WW, Hubbard A. 2005 Toward understanding the risk of secondary airborne infection: emission of respirable pathogens. *J. Occup. Environ. Hyg.* **2**, 143–154. (doi:10.1080/15459620590918466)
24. Johnson G *et al.* 2011 Modality of human expired aerosol size distributions. *J. Aerosol. Sci.* **42**, 839–851. (doi:10.1016/j.jaerosci.2011.07.009)
25. Yang S, Lee GW, Chen C-M, Wu C-C, Yu K-P. 2007 The size and concentration of droplets generated by coughing in human subjects. *J. Aerosol. Med.* **20**, 484–494. (doi:10.1089/jam.2007.0610)
26. Morawska L, Johnson G, Ristovski Z, Hargreaves M, Mengersen K, Corbett S, Chao CYH, Li Y, Katoshevski D. 2009 Size distribution and sites of origin of droplets expelled from the human respiratory tract during expiratory activities. *J. Aerosol. Sci* **40**, 256–269. (doi:10.1016/j.jaerosci.2008.11.002)
27. Zayas G, Chiang MC, Wong E, MacDonald F, Lange CF, Senthilselvan A, King M. 2012 Cough aerosol in healthy participants: fundamental knowledge to optimize droplet-spread infectious respiratory disease management. *BMC Pulm. Med.* **12**, 1–12. (doi:10.1186/1471-2466-12-11)
28. Scharfman B, Techet A, Bush J, Bourouiba L. 2016 Visualization of sneeze ejecta: steps of fluid fragmentation leading to respiratory droplets. *Exp. Fluids* **57**, 24. (doi:10.1007/s00348-015-2078-4)
29. Bahl P, Doolan C, de Silva C, Chughtai AA, Bourouiba L, MacIntyre CR. 2020 Airborne or droplet precautions for health workers treating COVID-19? *J. Infect. Dis.* (doi:10.1093/infdis/jiaa189)
30. Abkarian M, Mendez S, Xue N, Yang F, Stone HA. 2020 Speech can produce jet-like transport relevant to asymptomatic spreading of virus. *Proc. Natl Acad. Sci. USA* **117**, 25 237–25 245. (doi:10.1073/pnas.2012156117)
31. Bourouiba L. 2020 The fluid dynamics of disease transmission. *Annu. Rev. Fluid Mech.* **53**, 473–508. (doi:10.1146/annurev-fluid-060220-113712)
32. Fullmer WD, Higham JE, LaMarche CQ, Issangya A, Cocco R, Hrenya CM. 2020 Comparison of velocimetry methods for horizontal air jets in a semicircular fluidized bed of Geldart Group D particles. *Powder Technol.* **359**, 323–330. (doi:10.1016/j.powtec.2019.09.073)
33. Mella D, Brevis W, Higham J, Racic V, Susmel L. 2019 Image-based tracking technique assessment and application to a fluid–structure interaction experiment. *Proc. Instit. Mech. Eng. Part C* **233**, 5724–5734. (doi:10.1177/0954406219853852)
34. Lucas BD, Kanade T. 1981 An iterative image registration technique with an application to stereo vision. In *Proc. of the 7th Int. Conf. on Artificial Intelligence (IJCAI), Vancouver, British Columbia, Canada, 24–28 August 1981*, vol. 1, pp. 674–679.
35. Haffner EA, Mirbod P. 2020 Velocity measurements of a dilute particulate suspension over and through a porous medium model. *Phys. Fluids* **32**, 083608. (doi:10.1063/5.0015207)
36. Settles GS. 2012 *Schlieren and shadowgraph techniques: visualizing phenomena in transparent media*. Berlin, Germany: Springer Science & Business Media.
37. Lucas BD, Kanade T. 1985 Optical navigation by the method of differences. In *Proc. of 9th Int. Joint Conf.*

on Artificial Intelligence (IJCAI), Los Angeles, CA, August 1985, vol. 2, pp. 981–984.

38. Higham J, Brevis W. 2019 When, what and how image transformation techniques should be used to reduce error in particle image velocimetry data? *Flow Meas. Instrum.* **66**, 79–85. (doi:10.1016/j.flowmeasinst.2019.02.005)
39. Illingworth J, Kittler J. 1987 The adaptive Hough transform. *IEEE Trans. Pattern Anal. Mach. Intell.* **PAMI-9(no. 5)**, 690–698. (doi:10.1109/TPAMI.1987.4767964)
40. Sonkin LS. 1951 The role of particle size in experimental air-borne infection. *Am. J. Hyg.* **53**, 337–354.
41. Wells WF. 1955 *Airborne contagion and air hygiene. An ecological study of droplet infections*, pp. 1–19. Cambridge, MA: Harvard University Press.
42. Rosin P. 1933 Laws governing the fineness of powdered coal. *J. Inst. Fuel* **7**, 29–36.
43. Varga E, Titchener-Hooker N, Dunnill P. 2001 Prediction of the pilot-scale recovery of a recombinant yeast enzyme using integrated models. *Biotechnol. Bioeng.* **74**, 96–107. (doi:10.1002/bit.1099)
44. Lefebvre AH, McDonell VG. 2017 *Atomization and sprays*. Boca Raton, FL: CRC Press.
45. Dunbar CA, Hickey AJ. 2000 Evaluation of probability density functions to approximate particle size distributions of representative pharmaceutical aerosols. *J. Aerosol. Sci.* **31**, 813–831. (doi:10.1016/S0021-8502(99)00557-1)
46. Zigan L, Schmitz I, Wensing M, Leipertz A. 2012 Reynolds number effects on atomization and cyclic spray fluctuations under gasoline direct injection conditions. In *Fuel systems for IC engines*, pp. 253–263. Cambridge, UK: Woodhead Publishing.
47. van der Voort DD, Dam NJ, Clercx HJ, Van De Water W. 2018 Characterization of spray-induced turbulence using fluorescence PIV. *Exp. Fluids* **59**, 110. (doi:10.1007/s00348-018-2561-9)
48. Gupta J, Lin CH, Chen Q. 2009 Flow dynamics and characterization of a cough. *Indoor Air* **19**, 517–525. (doi:10.1111/j.1600-0668.2009.00619.x)
49. Bourouiba L, Dehandschoewercker E, Bush JW. 2014 Violent expiratory events: on coughing and sneezing. *J. Fluid Mech.* **745**, 537–563. (doi:10.1017/jfm.2014.88)
50. Wells WF. 1934 On air-borne infection: study II. Droplets and droplet nuclei. *Am. J. Epidemiol.* **20**, 611–618. (doi:10.1093/oxfordjournals.aje.a118097)
51. Sirignano WA. 2010 *Fluid dynamics and transport of droplets and sprays*. Cambridge, UK: Cambridge University Press.
52. Mittal R, Ni R, Seo J-H. 2020 The flow physics of COVID-19. *J. Fluid Mech.* **894**, F2-1-10. (doi:10.1017/jfm.2020.330)
53. Mittal R, Meneveau C, Wu W. 2020 A mathematical framework for estimating risk of airborne transmission of COVID-19 with application to face mask use and social distancing. *Phys. Fluids* **32**, 101903. (doi:10.1063/5.0025476)
54. Bazant MZ, Bush JWM. 2020 Beyond six feet: a guideline to limit indoor airborne transmission of COVID-19. See https://www.medrxiv.org/content/10.1101/2020.08.26.20182824v2.
55. Abkarian M, Stone H. 2020 Stretching and break-up of saliva filaments during speech: a route for pathogen aerosolization and its potential mitigation. *Phys. Rev. Fluids* **5**, 102301. (doi:10.1103/PhysRevFluids.5.102301)